Atmospheric Environment 141 (2016) 20–29

Contents lists available at ScienceDirect

Atmospheric Environment

journal homepage: www.elsevier.com/locate/atmosenv

Trans-boundary aerosol transport during a winter haze episode in China revealed by ground-based Lidar and CALIPSO satellite

Kai Qin [a], Lixin Wu [a, *], Man Sing Wong [b], Husi Letu [d], Mingyu Hu [a], Hongmei Lang [a], Shijie Sheng [c], Jiyao Teng [a], Xin Xiao [a], Limei Yuan [a]

[a] School of Environment Science and Spatial Informatics, China University of Mining and Technology, Xuzhou, China
[b] Department of Land Surveying and Geo-Informatics, The Hong Kong Polytechnic University, Kowloon, Hong Kong
[c] Wuxi CAS Photonics Corporation, Wuxi, China
[d] Institute of Remote Sensing and Digital Earth, Chinese Academy of Sciences, Beijing, China

HIGHLIGHTS

- A trans-boundary transport of aerosols during a large-area haze episode in China during 3–5 January 2015 was investigated.
- Pollutants moving from Hebei, Henan, and Hubei probably contributed to the haze pollution in Shandong and Jiangsu.
- A considerable amount of total optical depth below 3 km (46% in average) was contributed by the external aerosol layers
- Haze transports from North China Plain to East China could be a common phenomenon influenced by the winter monsoon.

ARTICLE INFO

Article history:
Received 28 January 2016
Received in revised form
30 May 2016
Accepted 16 June 2016
Available online 18 June 2016

Keywords:
Haze
$PM_{2.5}$
Aerosol
Lidar
CALIPSO
Trans-boundary transport

ABSTRACT

By employing $PM_{2.5}$ observation data, ground-based lidar measurements, MODIS and CALIPSO satellite images, meteorological data, and back trajectories analysis, we investigate a trans-boundary transport of aerosols during a large-area haze episode in China during 3–5 January 2015. The ground-based lidar observations indicated similar episodes of external aerosols passing through and mixing into three East China cities. A considerable amount of total AOD below 3 km (46% in average) was contributed by the external aerosol layers during passing over and importing. CALIPSO satellite observations of central and eastern China revealed a high altitude pollutant belt on January 3. Although the severest ground pollution was found in central and south-eastern Hebei, the high altitude pollution transport was greater in south-western Shandong, north-western Jiangsu, and north-western Anhui. These observations along with the analysis of air mass trajectories and wind fields indicates pollutants moving from Hebei, Henan and Hubei probably contributed to the haze pollution in Shandong and Jiangsu. This study reveals haze transports from North China Plain to East China could be a common phenomenon influenced by the winter monsoon in northern China. Hence, effective control of air pollution requires collaboration among different cities and provinces throughout China. The long-term measurements of aerosol vertical properties by ground-based lidar and CALIPSO are extremely valuable in quantifying the contributions of external factors and will be helpful in validating and improving various air quality models.

1. Introduction

With the rapid industrialization and urbanization in China, increasing anthropogenic emissions (Zhang et al., 2012a) during the last decades have significantly caused serious air pollution that adversely influences public health (Chen et al., 2013). In particular, prolonged regional haze events over large areas and high $PM_{2.5}$ (particulate matter with diameters less than 2.5 μm in aerodynamics) concentration have occurred frequently during autumn and winter in recent years. In January 2013, China experienced widespread haze with record-breaking $PM_{2.5}$ affecting hundreds of millions of citizen and covering most parts of central and eastern China. In some heavily polluted areas of Beijing, the highest instantaneous concentration of $PM_{2.5}$ reached 1000 μgm^{-3}

* Corresponding author.
E-mail address: awulixin@263.net (L. Wu).

http://dx.doi.org/10.1016/j.atmosenv.2016.06.042

(Zhang et al., 2014), which caused wide concern for both the public and government agencies. Thereafter, many researchers studied the physical, chemical, and optical properties of aerosol particles and meteorological conditions to understand the causes of the severe haze pollution in China (Che et al., 2014; Quan et al., 2014; Sun et al., 2014; Tao et al., 2014; Wang et al., 2014a, 2014b,d; Wang et al., 2014; Ji et al., 2014; Zhang et al., 2014). The main factors contributing to the formation of recent regional haze are (a) high secondary aerosol transformation from gaseous pollutants (Huang et al., 2014); (b) stable synoptic conditions with weak surface wind, vertical temperature inversion, and low PBL (planetary boundary layer) height (Wang et al., 2014e); and (c) trans-boundary regional transport (Zheng et al., 2015).

In September 2013, the China State Council announced the Air Pollution Prevention Plan to reduce the $PM_{2.5}$ level. This plan calls for urgent implementation of regional joint prevention and control measures to address the air pollution crisis effectively. Hence, understanding the trans-boundary transport of pollutants during the haze episodes is especially important for regional joint mitigation of air pollution in China. Wang et al. (2014a) used the NAQPMS (Nested Air Quality Prediction Model System) to investigate the contribution of BTH (Beijing, Tianjin, and Hebei) and surrounding areas to regional $PM_{2.5}$ distribution during 10–13 January 2013. They found the total transport contribution (trans-cluster transport outside BTH, plus inner transport inside BTH) was comparable to local emissions. Wang. et al. (2014c) used the MM5 (Mesoscale Modelling System Generation 5) and the CMAQ (Models-3/Community Multiscale Air Quality) modelling system to quantify the regional sources' contributions to the extreme haze pollution in January 2013 over three cities in Hebei. Using an online mesoscale haze forecasting model GRAPES-CUACE (Global/Regional Assimilation and PrEdiction System and the Chinese Unified Atmospheric Chemistry Environment), Jiang et al. (2015) showed that particulate matter imports from Beijing environment were much higher than the exports from the city during the severe haze episode on 6–7 December 2013.

However, previous studies relied on air quality models only to simulate and evaluate the regional haze movement in China. Only a few studies were based on direct observations. Lidar (light detection and ranging) technology, with the ability to detect aerosol vertical properties, has proven to be a very effective tool in detecting and tracking the transport of dust (Huang et al., 2008), volcanic plume (Revuelta et al., 2012), and wildfire smoke (Wu et al., 2012; Cottle et al., 2014). Here, we report a trans-boundary transport during a haze episode in China in January 2015, using both ground-based lidar detections and CALIPSO (Cloud-Aerosol lidar and Infrared Pathfinder Satellite Observations) satellite observation. MODIS (MODerate resolution Imaging Spectroradiometer) images and $PM_{2.5}$ data were collected to describe the loading and spatial distribution of the haze episode. In additional, metrological conditions and back trajectories were analyzed to identify the transport pathway and pollutant source.

2. Data and method

2.1. Ground-based lidar measurements

Ground-based lidar measurements in three East China cities (Xuzhou, Wuxi, and Fuzhou, indicated as yellow stars in Fig. 2) were collected in this study. A mini micro pulse lidar system (model MiniMPL) manufactured by Sigma Space Corporation was installed at the air quality monitoring site (34.22° N, 117.14° E, 60 m) of CUMT (China University of Mining and Technology), Xuzhou City, Jiangsu Province, to conduct experimental observations in January 2015. The MiniMPL is a portable version of micro pulse lidar deployed in the NASA global lidar network (MPLNET). It emits green light at 532 nm with energy of 3–4 μJ at 532 nm and a pulse repetition rate of 2500 Hz. Its time resolution is 30-s and the vertical resolution is 30 m. The zone of incomplete afterpulse correction (overlap area) is approximately 120 m. A high-energy lidar system (model AGHJ-I-LIDAR), manufactured by Wuxi CAS Photonics Corporation, has been operated at China Sensor Network Innovation Park (31.5° N, 120.37° E, 10 m), Wuxi City, Jiangsu Province, since 2011. In January 2015, another AGHJ-I-LIDAR was installed at Fuzhou Environmental Information Center (26.09° N, 119.32° E, 15 m), Fuzhou City, Fujian Province, to conduct experimental observations. The AGHJ-I-LIDAR also emits green light at 532 nm but with energy of 20 mJ and a pulse repetition rate of 20 Hz. Its time resolution is 1-min and the vertical resolution is 7.5 m. The overlap area is approximately 300 m. For both MiniMPL and AGHJ-I-LIDAR, the raw measurements with a high-temporal resolution were averaged in 5-min intervals to improve signal-to-noise ratio for deriving aerosol-extinction profiles by solving the lidar equation with a traditional Fernald algorithm (Fernald, 1984). More details about the data processing of the two lidar systems can be found in Campbell et al. (2002) and Liu et al. (2007), respectively.

2.2. Satellite dataset

The MODIS aboard Terra and Aqua satellites pass China twice every day around 11:00 and 13:00 local time and capture data in 36 spectral bands, ranging from 0.4 μm to 14.4 μm. MODIS true-colour images provide a synoptic view of the spatial extent of haze pollution (Tao et al., 2014). AOD (Aerosol optical depth) retrieved from MODIS spectra data has been widely used in climate and air quality studies (Wong et al., 2010, 2011; Pappas et al., 2013; Li et al., 2013; 2015; Bai et al., 2016). MODIS-Aqua true-colour images and AOD data during 3–5 January 2015 were used to obtain the spatial extent and intensity of this haze episode.

In 2006, the CALIPSO satellite was launched in a sun-synchronous polar orbit around the Earth as part of the "A-train" constellation of Earth observing satellites. CALIOP (Cloud-Aerosol lidar with Orthogonal Polarization), loaded on CALIPSO, is a dual-wavelength (532 nm and 1064 nm), dual-polarization, elastic backscatter lidar. One of the most distinct advantages of CALIPSO lidar detection is that it provides a direct measurement of the vertical structure and optical properties of aerosols at both regional and global scales (Winker et al., 2007, 2009). Three types of images, including 532 nm TABC (total attenuated backscatter coefficient), VFM (vertical feature masks), and AS (aerosol subtype), from the CALIPSO website (http://www-calipso.larc.nasa.gov/) were used in this study. The 532 nm TABC image from CALIPSO level 1b data is the sum of 532 nm parallel and perpendicular return signals and has been colour-coded such that blue corresponds to molecular scattering and weak aerosol scattering and yellow/red/orange show the increase of aerosol loadings. The VFM image from CALIPSO level 2 data (Burton et al., 2013) shows the vertical and horizontal distribution of cloud and aerosol layers in terms of different feature types, such as clear air, cloud, aerosol, stratospheric feature, surface, subsurface, and no signal (totally attenuated). The AS image from CALIOP level 2 data shows the vertical and horizontal distribution of different aerosol subtypes, such as clean marine, dust, polluted continental, clean continental, polluted dust, and smoke (Mielonen et al., 2009).

2.3. $PM_{2.5}$ and meteorological data

In February 2012, China's Ministry of Environmental Protection approved the technical regulation of the ambient air quality index (on trial, GB 3095-2012), which released $PM_{2.5}$ values to the public

for the first time. The National Real-Time Air Quality Reporting System released by the China National Environmental Monitoring Center now publishes hourly concentration of $PM_{2.5}$ in most cities at prefecture level and above (http://106.37.208.233:20035/). The daily concentrations of $PM_{2.5}$ (24-h average of hourly data) in 367 cities in China were used to characterize the severe pollution of China in January 2015.

The hourly changes of $PM_{2.5}$, visibility, and relative humidity and wind speed in Xuzhou were compared with the lidar-derived aerosol-extinction profiles to reveal the effect of trans-regional aerosol transport on local haze pollution. The data were measured by an aerosol particle analyzer (model Grimm 180), a visibility sensor (model Belfort Model 6000), and a weather station (model Davis Vantage Pro2) equipped at the air quality monitoring site of CUMT.

The wind field data from NCEP (National Centers for Environmental Prediction), Final Analysis data (1° × 1°, 6-hourly; NCEP-FNL; http://rda.ucar.edu/datasets/ds083.2/), were used to analyze the meteorological conditions during the haze episode. Backward trajectories of air mass were analyzed using the HYSPLIT (Hybrid Single-Particle Lagrangian Integrated Trajectory) (http://ready.arl.noaa.gov/HYSPLIT.php) to track air mass transports during the haze episode.

3. Results and analysis

3.1. General view of the haze pollution in China during 3–5 January 2015

Fig. 1 was generated by spatial interpolation of daily $PM_{2.5}$ concentration in 367 cities, in which widespread haze pollution covered most of central and eastern China. The spatial distribution of the haze extended and the loadings increased gradually from 3 to 5 January 2015. The most polluted region was the NCP (North China Plain, including central and southern Hebei, northern Henan, western Shandong, and northern Jiangsu), eastern Sichuan, and central Hubei. The 10 cities with the highest daily $PM_{2.5}$ concentration were indicated as blue points in Fig. 1, of which, five cities were in Hebei (Xingtai, Baoding, Shijiazhuang, Handan, and Hengshui), three cities were in Henan (Anyang, Zhengzhou, and Jiaozuo), one city was in Hubei (Yichang), and one was in Sichuan (Dazhou). The highest daily $PM_{2.5}$ concentration of 489 μgm^{-3} was recorded in Baoding on 4 January (Table 1). Aqua MODIS true-colour images in Fig. 2a–b shows that gray haze plumes appeared over NCP in the afternoon of 3 January, and then obscured the surface of most of the central and eastern China in the afternoon of 4 January. Aqua MODIS AOD data in Fig. 2c–d shows most of the haze plumes exhibited strong aerosol loadings with high AOD (greater than 0.9) in the afternoons of 3 and 4 January.

3.2. External aerosol layers in three east China cities detected by ground-based lidar

Fig. 3 shows the time-height cross section of the ground-based lidar-derived extinction coefficient at 532 nm during 3–5 January 2015 in Xuzhou, Wuxi, and Fuzhou. The effective detection range of aerosol layer from both AGHJ-I-LIDAR and MiniMPL were around 3 km, screening for clouds and noises. Both in Xuzhou and Wuxi, there were two episodes of external aerosols passing over and mixing downward into the local PBLs. In Xuzhou, the first external aerosol layer arrived at 0:00 (local time) on 3 January at 1–3 km altitude under clouds; it subsequently mixed downward into the PBL from 15:00 on 3 January; then the second one arrived and mixed into the PBL along with the descending clouds on 5 January. In Wuxi, both the two external aerosol layers appeared later with similar intensities but lower altitudes as compared to Xuzhou. In Fuzhou, the external aerosol layer with significantly weaker intensities was identifiable from 13:00 on 3 January and then mixed downward into the PBL; on 5 January, there were only a few aerosols under the clouds which did not reach the PBL.

To quantitatively assess the contribution of trans-boundary aerosols, we calculated the total AOD below 3 km and separated it into local and external components. The local and external AOD were calculated by integrated the extinction coefficient profiles in 0.12/0.2 (MiniMPL/AGHJ-I-LIDAR)-1 km and 1–3 km, respectively. We further defined the external aerosol fraction (EAF) as the sum of external AOD divided by the sum of total AOD below 3 km during the external aerosols passing over and importing. As shown in

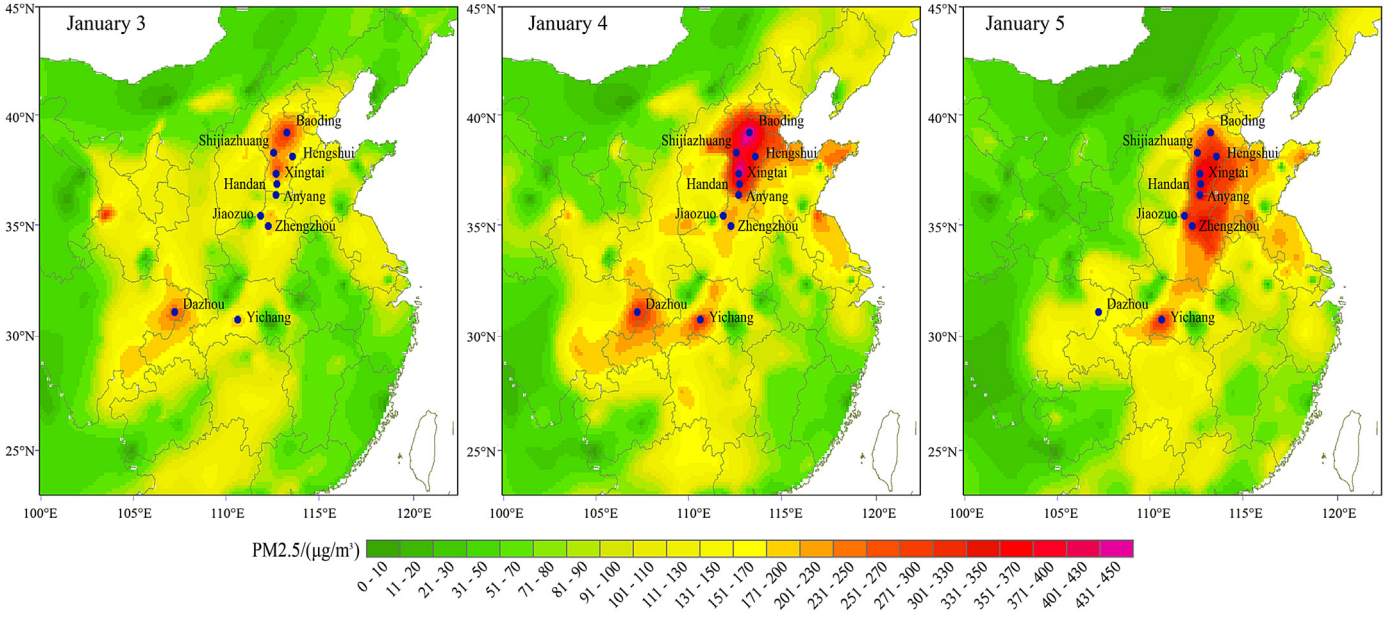

Fig. 1. Spatial distribution of daily $PM_{2.5}$ in central and eastern China.

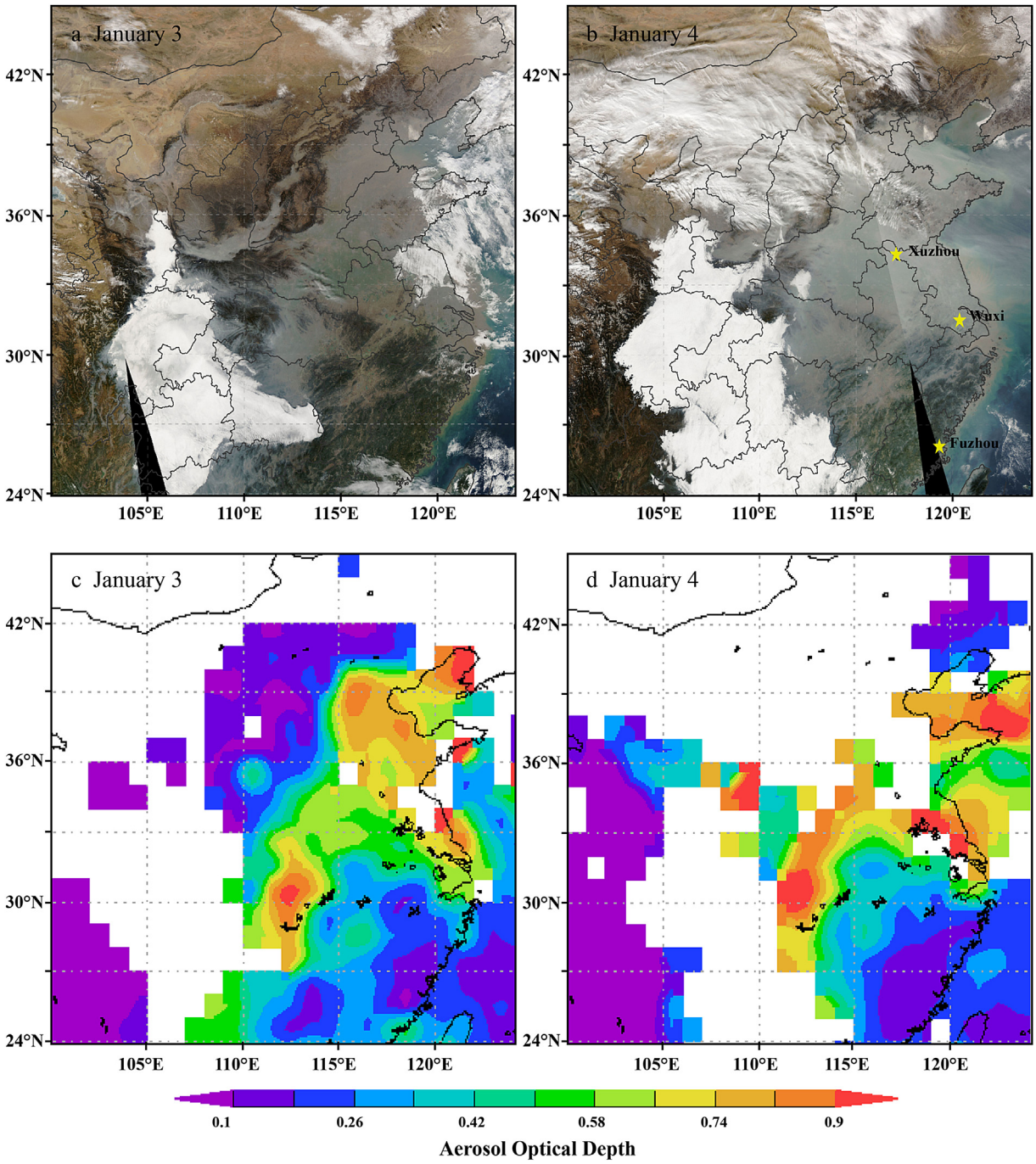

Fig. 2. Aqua MODIS true colour images and AOD of central and eastern China.

Table 1
Daily $PM_{2.5}$ concentration (unit in μgm^{-3}) in top 10 most polluted cities during 3–5 January 2015.

	Hebei					Henan			Hubei	Sichuan
	Xingtai	BaoDing	Hengshui	Shijiazhuang	Handan	Jiaozhuo	Zhengzhou	Anyang	Yichang	Dazhou
3 Jan 2015	281	315	172	234	156	151	194	133	204	268
4 Jan 2015	484	489	324	386	372	225	231	327	306	323
5 Jan 2015	416	260	346	269	334	327	335	469	324	166

Fig. 4, the local AODs in all the three cities became larger to different degrees (Table 2) after the external aerosols reached the PBL, demonstrating the interaction between external aerosols and local pollutants. Taking Xuzhou for example, for the first external aerosol layer, the average local AOD was 0.14 during the period of passing over but without importing (0:00–14:00, 3 January), while

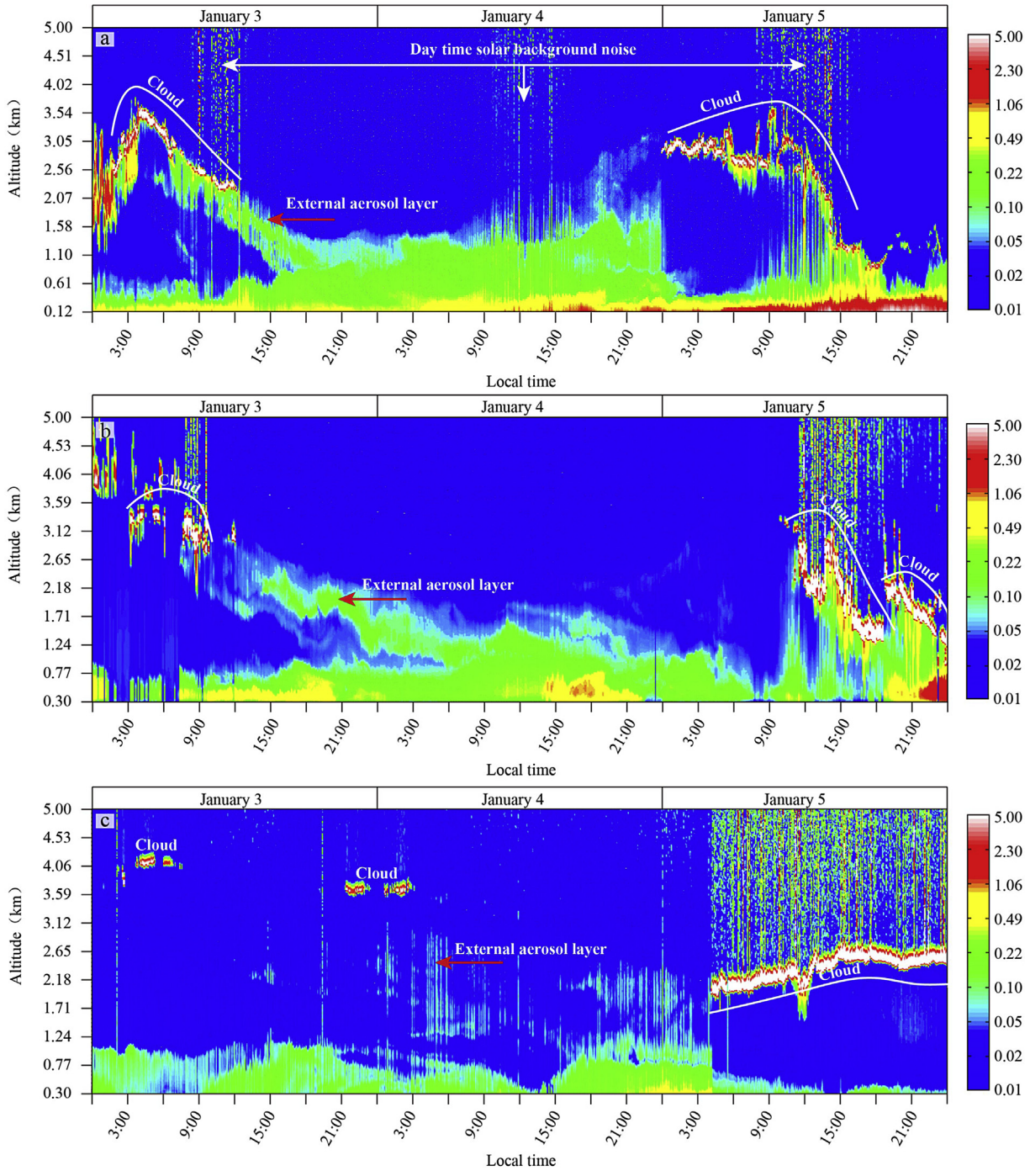

Fig. 3. Time-height cross section of the ground-based lidar-derived extinction coefficient at 532 nm in Xuzhou (panel a), Wuxi (panel b), and Fuzhou (panel c). The colours were assigned in terms of a logarithm of the extinction coefficient.

it was 0.26 during the period of importing (15:00, 3 January-23:00, 4 January). The average EAF for the three sites is 0.46 (0.32–0.69), indicating a considerable amount of AOD contributed by the external aerosol layers.

To further understand the effect of the aerosol transport on local air quality, the hourly changes of $PM_{2.5}$ concentration, as well as surface meteorological variables (such as visibility, relative humidity, and wind speed), in Xuzhou were investigated, as shown in Fig. 5. Together with the vertical structure evolution of the lidar-derived extinction coefficient (Fig. 3a), it can be seen that $PM_{2.5}$ concentration rose almost linearly while the external aerosol layer reached and gradually mixed with the PBL after 15:00 on 3 January. Accordingly, the visibility decreased continuously over dozens of hours. In the afternoon of 5 January, $PM_{2.5}$ concentration slightly decreased as the ending of the external import. Whereas, the visibility continued to degrade as the relative humidity increased. In additional, the evolution of the PBL was weak (Fig. 3a) and the average wind speed was low (1.24 ms^{-1}, see Fig. 5) during the whole haze period.

In Fig. 6, the backward trajectories of air mass defining Xuzhou,

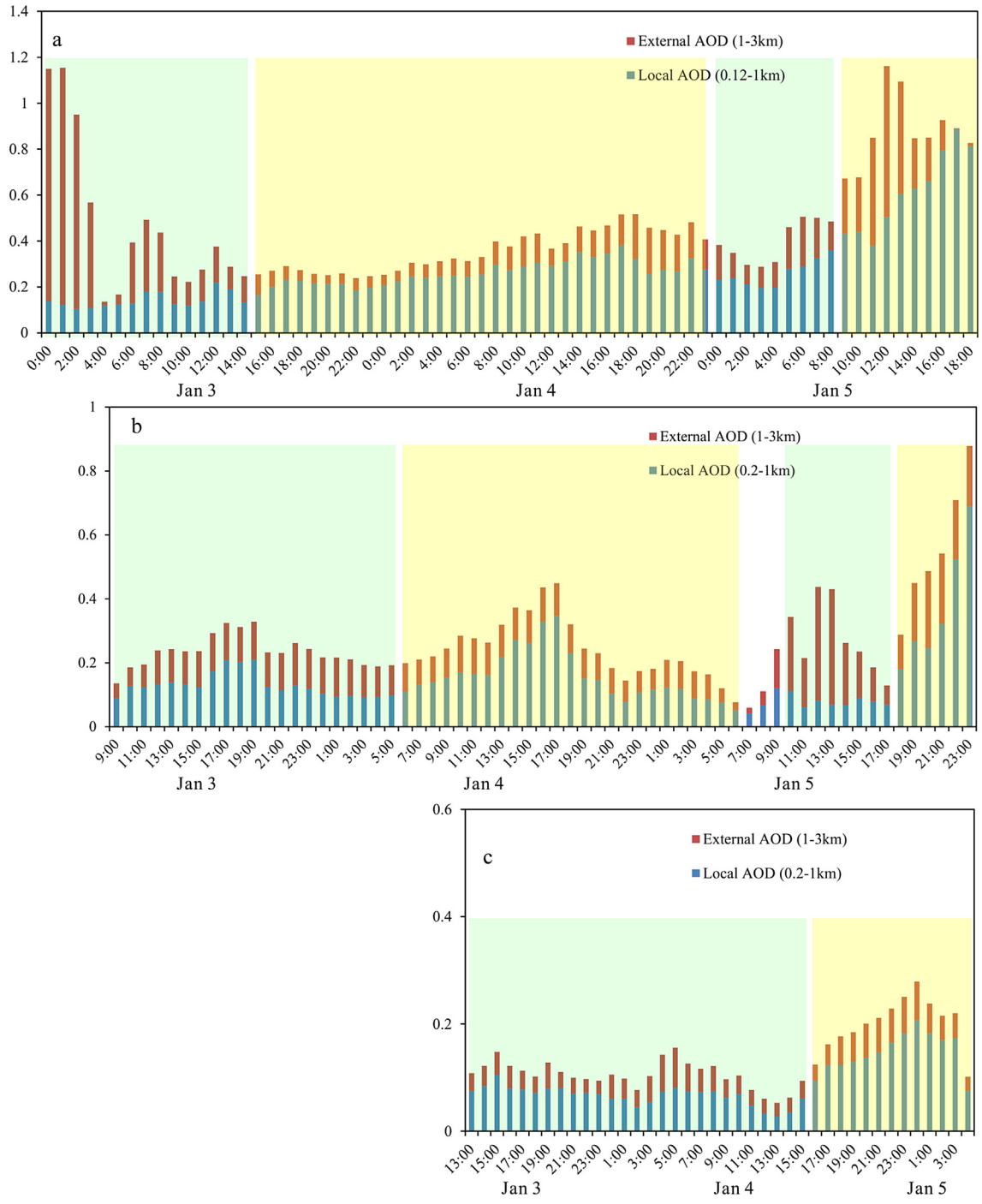

Fig. 4. Time series of local and external AOD in Xuzhou (panel a), Wuxi (panel b), and Fuzhou (panel c). The green and yellow shadows represent the time periods of external aerosols passing over and importing, respectively. (For interpretation of the references to colour in this figure legend, the reader is referred to the web version of this article.)

Table 2
Statistics of the local AOD changes and the external aerosol fraction (EAF). #1 and #2 represent the first and second external aerosol layer, respectively. The time periods before (passing over) and after external importing can be seen in Fig. 4.

	Average local AOD before external importing	Average local AOD after external importing	EAF
Xuzhou #1	0.14	0.26	0.43
Xuzhou #2	0.26	0.62	0.69
Wuxi #1	0.13	0.16	0.39
Wuxi #2	0.08	0.37	0.49
Fuzhou #1	0.07	0.15	0.32

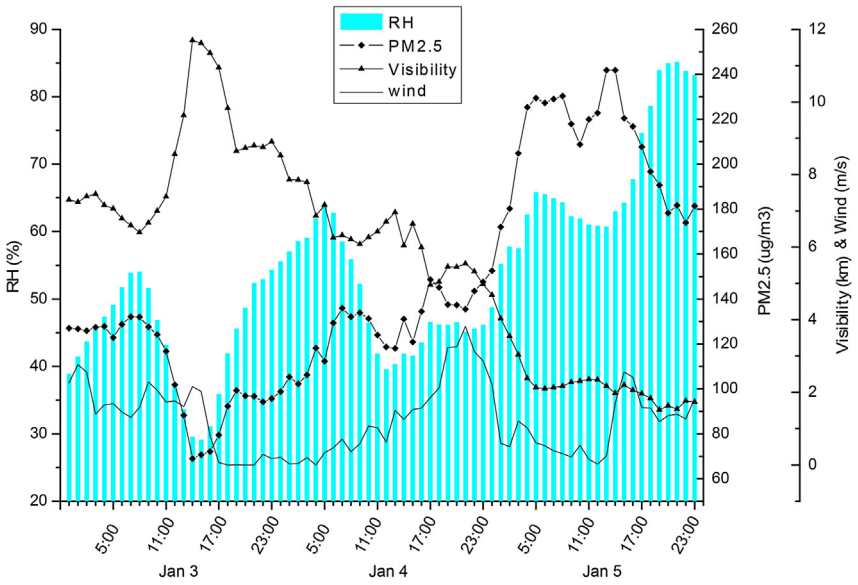

Fig. 5. Hourly $PM_{2.5}$, visibility, relative humidity, and wind speed from 3 to 5 January 2015 in Xuzhou.

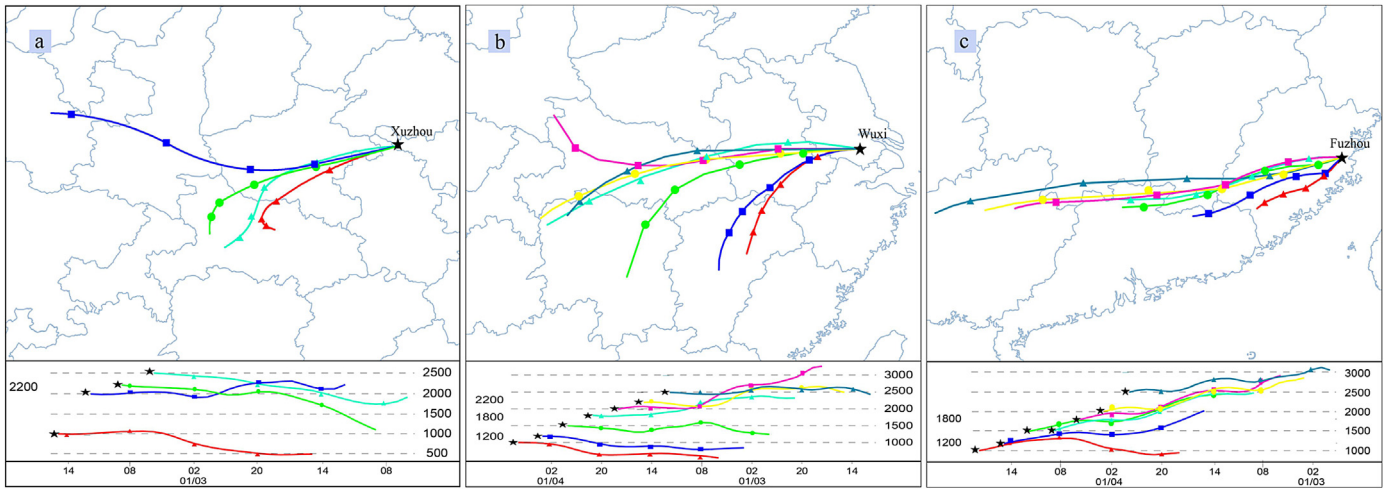

Fig. 6. 24-h backward trajectories of air mass in Xuzhou (panel a), Wuxi (panel b), and Fuzhou (panel c), calculated at specific heights and ending at specific times during the external aerosol pass through and import process.

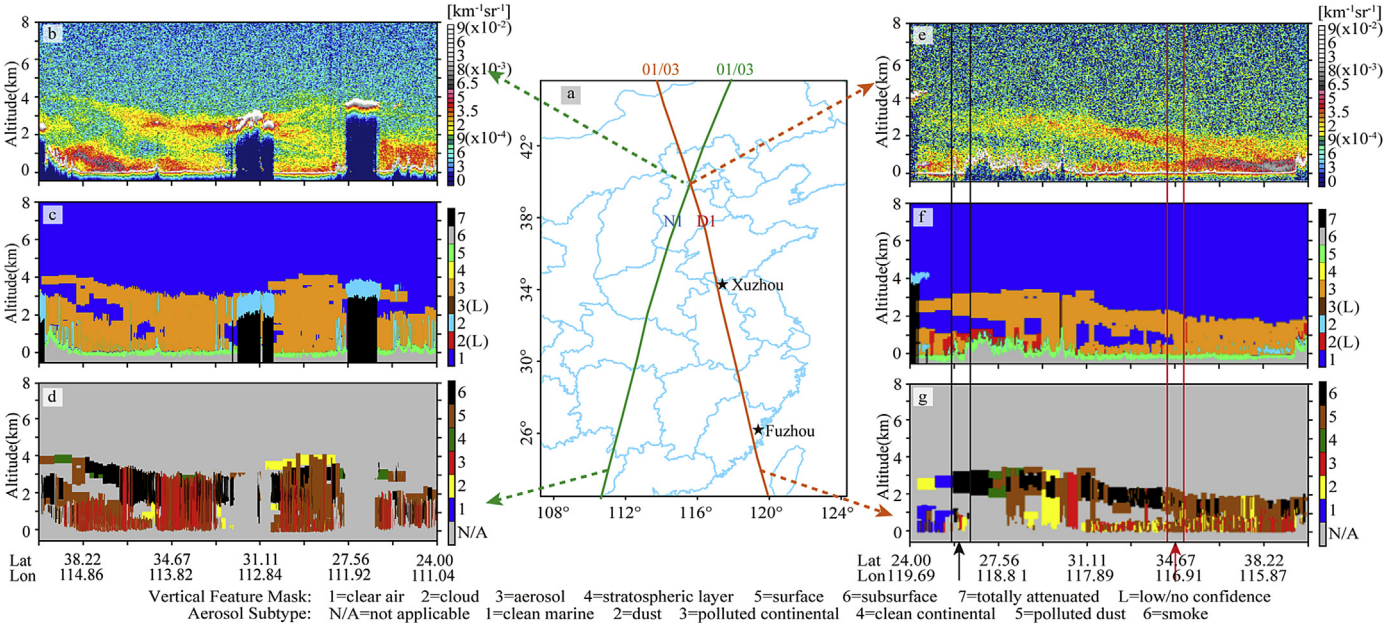

Fig. 7. CALIPSO 523 nm total attenuated backscatter coefficient, vertical feature masks, and aerosol subtype of nighttime (left) and daytime (right) orbits and ground-tracks (middle) on 3 January 2015. Red and black arrows indicate the locations of Xuzhou and Fuzhou, respectively. (For interpretation of the references to colour in this figure legend, the reader is referred to the web version of this article.)

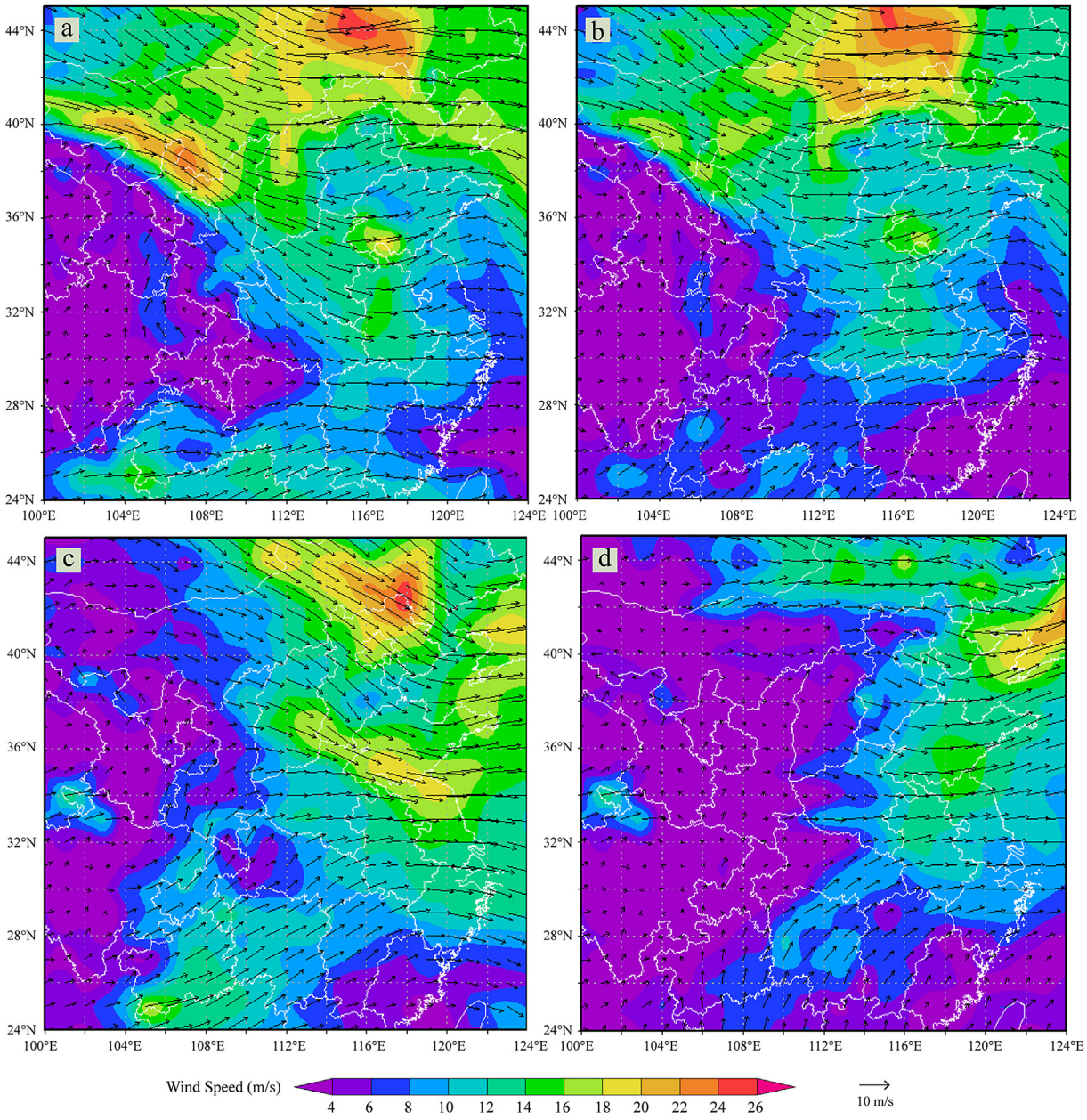

Fig. 8. 700 hPa (panel a) and 750 hPa (panel b) wind fields corresponding to the high altitude pollutant belt at 2–4 km at 2:00 on 3 January 2015; 750 hPa (panel c) and 850 hPa (panel d) wind fields corresponding to the high altitude pollutant belt at 1–3 km at 14:00 on 3 January 2015.

Wuxi, and Fuzhou as the terminal points were drawn in every 3 h at specific heights and times according to the ground-based lidar observations in Fig. 3. In general, the trajectories terminating at Xuzhou passed over Henan while the trajectories terminating at Wuxi largely passed over Hubei and Anhui. The airflows passed over severely polluted regions in Henan and Hubei including Zhengzhou and Yichang as two of the top 10 cities. Thus, those airflows probably transported external pollutants from Henan and Hubei to Xuzhou and Wuxi. The trajectories terminating at Fuzhou originated and passed over slightly polluted regions. Hence, the signals of external aerosol layer in Fig. 3c were weak.

3.3. *Trans-boundary aerosol transport observed by CALIPSO satellite*

Fig. 7a shows the CALIPSO satellite passing over central and eastern China twice on 3 January 2015. The blue line (N1) represents the upward orbit track during night ~2:30, while the red line (D1) represents the downward orbit track during the day ~13:30. The altitude-orbit cross section images of 532 nm TABC, VFM, and AS along the two orbit tracks (N and D1) are shown on the left and right panels in Fig. 7, respectively. Most of these images show clear two-layer structures. In addition to the local pollution layers near the ground, there were high altitude pollutant belts at 2–4 km (for N1) and 1–3 km (for D1) respectively. They were classified as aerosol in VFM and further as smoke in AS. The N1 swept across southern Hebei, central Henan, and north-central Hubei in which strong aerosol-extinction layers were found at both ground and high altitudes (Fig. 7b). The severest ground pollution was found in central and south-western Hebei. The D1 swept across Fuzhou and Xuzhou in which the aloft pollutant belt showed enhanced intensities at decreasing altitudes from south to north (Fig. 7e). In

Xuzhou, the aloft aerosol layer had similar intensities as the ground layer, which was consistent with the ground-based lidar observation (Fig. 3a). By contrast, the aloft aerosol layer in Fuzhou at a higher altitude was so weak that it was difficult to be detected by the ground lidar (Fig. 3c). Although the severest ground pollution was found in central and south-eastern Hebei, the high altitude pollution transports were more considerable in south-western Shandong, north-western Jiangsu, and north-western Anhui.

Fig. 8 displays the NCEP-FNL high altitude wind fields at 2:00 (around the time of N1 passing) and 14:00 (around the time of D1 passing) on 3 January. North-westerly winds with a velocity range of 16–26 ms^{-1} prevailed in most polluted provinces at 700 hPa (~3 km) at 2:00 (Fig. 8a). A north-westerly airflow in North China and a south-westerly airflow in South China were found at 750 hPa (~2.5 km) at 2:00 (Fig. 8b) and 14:00 (Fig. 8c), respectively. The 850 hPa (~1.5 km) wind field at 14:00 showed that the winds in eastern China were mostly travelled from west (Fig. 8d). Such a wind field configuration favours the transport of pollutants from Hebei and Henan to Shandong and from Hubei and Henan to Jiangsu by way of Anhui.

4. Summary

In this paper, trans-boundary aerosol transports during a haze episode in China in January 2015 were investigated using $PM_{2.5}$ observation data, ground lidar detections, MODIS images, CALIPSO satellite observations, meteorological data, and a back-trajectories analysis. The results are summarized as follows.

First, a large-area haze episode with high $PM_{2.5}$ concentration and AOD occurred in central and eastern China during 3–5 January 2015. Besides the widely reported haze in the NCP, severe pollution also occurred in eastern Sichuan and central Hubei. Second, the ground-based lidar observations in three East China cities (Xuzhou, Wuxi, and Fuzhou) revealed similar episodes of external aerosol passing over and mixing downward into the local PBLs during the haze period. These layers affected aerosol loadings in the local PBL to different degrees. A considerable amount of total aerosol optical depth below 3 km (46% in average) was contributed by the external aerosol layers during passing over and importing. The analysis of $PM_{2.5}$ as well as meteorological variables in Xuzhou demonstrated that both external import and weather conditions unfavorable to pollutant diffusion contributed to the local haze episode. Third, the CALIPSO satellite observations revealed that a high altitude pollutant belt existed both during night and day of January 3. The high altitude pollution transport was more considerable in south-western Shandong, north-western Jiangsu, and north-western Anhui. The analysis of backward trajectories and high altitude wind fields showed prevailing westerly airflow in most polluted areas. These facts indicate the transport of pollutants from Hebei, Henan, and Hubei probably contributed to the haze pollution in Shandong and Jiangsu.

In this case, the lidar technology with the ability to detect aerosol vertical properties makes it possible to reveal the haze's trans-boundary transport. Further studies with more haze cases are needed for quantifying the long-term contributions of external import, using an integrated method combining lidar observations, backward trajectories, and potential source contribution function (PSCF) modelling (Wong et al., 2013). Currently, increasingly more ground-based lidar measurements are being conducted by the state and local environmental protection and meteorological departments in China. Such measurements will be helpful in validating and improving various air quality models and further supporting the air pollution prevention plan. Under the influence of the winter monsoon in northern China, the trans-boundary aerosol transport across the two major haze areas (the NCP and East China; Zhang et al., 2012b) is possibly a common phenomenon during the frequent haze events. These findings suggest the effective control of air pollution requires collaboration, not only among cities within a city cluster, but also among multiple city clusters throughout China.

Acknowledgments

This study was supported by the Fundamental Research Funds for the Central Universities (2015XKMS049). We thank the MAESTRO (Mining Area Environment Synergic observaTion pRoving ground) program of CUMT for providing lidar data in Xuzhou. We thank the Sigma Space Corporation and the Wuxi CAS Photonics Corporation for providing lidar instruments. We thank the CALIPSO, MODIS mission scientists and associated NASA personnel for the production of the data used in this research effort. Analyses and visualizations used in this paper were produced with the Giovanni online data system, developed and maintained by the NASA GES DISC. We thank the NOAA Air Resources Laboratory (ARL) for the provision of the HYSPLIT transport and dispersion model and/or READY website (http://www.ready.noaa.gov) used in this publication. We thank Dr. Xu Jian from German Aerospace Center for help in improving the language.

References

Burton, S.P., Ferrare, R.A., Vaughan, M.A., et al., 2013. Aerosol classification from airborne HSRL and comparisons with the CALIPSO vertical feature mask. Atmos. Meas. Tech. 6 (5), 1397–1412.
Bai, Y., Wu, L., Qin, K., et al., 2016. A Geographically and temporally weighted regression model for ground-level PM2. 5 Estimation from satellite-derived 500 m resolution AOD. Remote Sens. 8 (3), 262.
Chen, Y., Ebenstein, A., Greenstone, M., et al., 2013. Evidence on the impact of sustained exposure to air pollution on life expectancy from China's Huai River policy. Proc. Natl. Acad. Sci. 110 (32), 12936–12941.
Cottle, P., Strawbridge, K., McKendry, I., 2014. Long-range transport of Siberian wildfire smoke to British Columbia: lidar observations and air quality impacts. Atmos. Environ. 90, 71–77.
Che, H., Xia, X., Zhu, J., et al., 2014. Aerosol optical properties under the condition of heavy haze over an urban site of Beijing. China. Environ. Sci. Pollut. Res. 1–11.
Campbell, J.R., Hlavka, D.L., Welton, E.J., et al., 2002. Full-time, eye-safe cloud and aerosol lidar observation at atmospheric radiation measurement program sites: instruments and data processing. J. Atmos. Ocean. Technol. 19 (4), 431–442.
Fernald, F.G., 1984. Analysis of atmospheric lidar observations- Some comments. Appl. Opt. 23 (5), 652–653.
Huang, J.P., Patrick, M., Chen, B., et al., 2008. Long-range transport and vertical structure of Asian dust from CALIPSO and surface measurements during PACDEX. J. Geophys. Res. 113 (D23).
Huang, R., Zhang, Y., Bozzetti, C., et al., 2014. High secondary aerosol contribution to particulate pollution during haze events in China. Nature 514 (7521), 218–222.
Ji, D.S., Li, L., Wang, Y.S., et al., 2014. The heaviest particulate air-pollution episodes occurred in northern China in January, 2013: insights gained from observation. Atmos. Environ. 92, 546–556.
Jiang, C., Wang, H., Zhao, T., et al., 2015. Modeling study of PM 2.5 pollutant transport across cities in China's Jing–Jin–Ji region during a severe haze episode in December 2013. Atmos. Chem. Phys. 15 (10), 5803–5814.
Liu, B., Zhong, Z., Zhou, J., 2007. Development of a Mie scattering lidar system for measuring whole tropospheric aerosols. J. Opt. A Pure Appl. Opt. 9 (10), 828–832.
Li, S, Chen, L, Xiong, X, et al., 2013. Retrieval of the haze optical thickness in North China Plain using MODIS data. IEEE Trans. Geosci. Remote Sens. 51 (5), 2528–2540.
Li, S, Kahn, R, Chin, M, et al., 2015. Improving satellite-retrieved aerosol microphysical properties using GOCART data. Atmos. Meas. Tech. 8 (3), 1157–1171.
Mielonen, T., Arola, A., Komppula, M., et al., 2009. Comparison of CALIOP level 2 aerosol subtypes to aerosol types derived from AERONET inversion data. Geophys. Res. Lett. 36 (18).
Pappas, V., Hatzianastassiou, N., Papadimas, C., et al., 2013. Evaluation of spatiotemporal variability of Hamburg Aerosol Climatology against aerosol datasets from MODIS and CALIOP. Atmos. Chem. Phys. 13 (16), 8381–8399.
Quan, J., Tie, X., Zhang, Q., et al., 2014. Characteristics of heavy aerosol pollution during the 2012–2013 winter in Beijing, China. Atmos. Environ. 88, 83–89.
Revuelta, M.A., Sastre, M., Fernández, A.J., et al., 2012. Characterization of the Eyjafjallajökull volcanic plume over the Iberian Peninsula by lidar remote sensing and ground-level data collection. Atmos. Environ. 48, 46–55.
Sun, Y., Jiang, Q., Wang, Z., et al., 2014. Investigation of the sources and evolution processes of severe haze pollution in Beijing in January 2013. J. Geophys. Res. 119 (7), 4380–4398.

Tao, M., Chen, L., Xiong, X., et al., 2014. Formation process of the widespread extreme haze pollution over northern China in January 2013: implications for regional air quality and climate. Atmos. Environ. 98, 417–425.
Wu, Y., Cordero, L., Gross, B., et al., 2012. Smoke plume optical properties and transport observed by a multi-wavelength lidar, sunphotometer and satellite. Atmos. Environ. 63, 32–42.
Wang, Z.F., Jie, L., Zhe, W., et al., 2014a. Modeling study of regional severe hazes over mid-eastern China in January 2013 and its implications on pollution prevention and control. Sci. China Earth Sci. 57 (1), 3–13.
Wang, H., Tan, S.-C., Wang, Y., et al., 2014b. A multisource observation study of the severe prolonged regional haze episode over eastern China in January 2013. Atmos. Environ. 89 (0), 807–815.
Wang, L.T., Wei, Z., Yang, J., et al., 2014c. The 2013 severe haze over southern Hebei, China: model evaluation, source apportionment, and policy implications. Atmos. Chem. Phys. 14, 3151–3173.
Wang, H., Xu, J., Zhang, M., et al., 2014d. A study of the meteorological causes of a prolonged and severe haze episode in January 2013 over central-eastern China. Atmos. Environ. 98, 146–157.
Wang, Y.S., Yao, L., Wang, L.L., et al., 2014e. Mechanism for the formation of the January 2013 heavy haze pollution episode over central and eastern China. Sci. China Earth Sci. 57 (1), 14–25.
Wong, M.S., Lee, K.H., Nichol, J.E., et al., 2010. Retrieval of aerosol optical thickness using MODIS 500 x 500m^2, a study in Hong Kong and pearl river delta region. IEEE Trans. Geosci. Remote Sens. 48 (8), 3318–3327.
Wong, M.S., Nichol, J.E., Lee, K.H., 2011. An operational MODIS aerosol retrieval algorithm at high spatial resolution, and its application over a complex urban region. Atmos. Res. 99 (3–4), 570–589.
Wong, M.S., Nichol, J.E., Lee, K.H., 2013. Estimation of aerosol sources and aerosol transport pathways using AERONET clustering and backward trajectories: a case study of Hong Kong. Int. J. Remote Sens. 34 (3), 938–955, 2013.
Winker, D.M., Hunt, W.H., McGill, M.J., 2007. Initial performance assessment of CALIOP. Geophy. Res. Lett. 34 (19) http://dx.doi.org/10.1029/2007GL030135.
Winker, D.M., Vaughan, M.A., Omar, A., et al., 2009. Overview of the CALIPSO mission and CALIOP data processing algorithms. J. Atmos. Ocean. Tech. 26 (11), 2310–2323.
Zhang, Q., He, K., Huo, H., 2012a. Policy: cleaning China's air. Nature 484 (7393), 161–162.
Zhang, X.Y., Wang, Y.Q., Niu, T., et al., 2012b. Atmospheric aerosol compositions in China: spatial/temporal variability, chemical signature, regional haze distribution and comparisons with global aerosols. Atmos. Chem. Phys. 12 (2), 779–799.
Zhang, J.K., Sun, Y., Liu, Z.R., et al., 2014. Characterization of submicron aerosols during a month of serious pollution in Beijing, 2013. Atmos. Chem. Phys. 14 (6), 2887–2903.
Zheng, G.J., Duan, F.K., Su, H., et al., 2015. Exploring the severe winter haze in Beijing: the impact of synoptic weather, regional transport and heterogeneous reactions. Atmos. Chem. Phys. 15 (6), 2969–2983.